Chapter 1

Quadrupole Moment and Tensor Force

“The mixing of ℓ values in the deuteron is the best evidence we have for the noncentral (tensor) character of the nuclear force.”

K. S. Krane

1.1 Electric quadrupole moment from the multipole expansion

The magnetic moment of the deuteron is close to, but not equal to, the sum of the free nucleon moments. That small discrepancy already suggests a few percent D-wave admixture. A sharper geometric probe is the electric quadrupole moment: it reports the *shape* of the charge distribution. The definition used in nuclear physics follows from the multipole expansion of the electrostatic potential of a localised charge density, exactly as in the original lecture (Fig. 1 below) [6, 1, 2].

1.1.1 Potential of a nuclear charge distribution (Fig. 1)

Let $\rho(\boldsymbol{r}')$ be the charge density of the nucleus. The electric potential at an exterior point $\boldsymbol{r}$ is

$$\Phi(\boldsymbol{r}) = \frac{1}{4\pi\varepsilon_0} \int \frac{\rho(\boldsymbol{r}')}{|\boldsymbol{r} - \boldsymbol{r}'|} \, \mathrm{d}^3 r', \tag{1.1}$$

where $\boldsymbol{r}'$ labels a charge element inside the nucleus (Figure 1.1).

1.1.2 Multipole expansion far from the nucleus

Far from the nucleus one expands the Coulomb kernel in Legendre polynomials. Write

$$|\boldsymbol{r} - \boldsymbol{r}'| = r \left(1 - 2\frac{r'}{r} \cos\theta + \left(\frac{r'}{r}\right)^2 \right)^{1/2},$$

with θ the angle between $\boldsymbol{r}$ and $\boldsymbol{r}'$. For $r > r'$ the generating function of Legendre polynomials is

$$\frac{1}{|\boldsymbol{r} - \boldsymbol{r}'|} = \frac{1}{r} \sum_{\ell=0}^{\infty} \left(\frac{r'}{r}\right)^{\ell} P_\ell(\cos\theta). \tag{1.2}$$

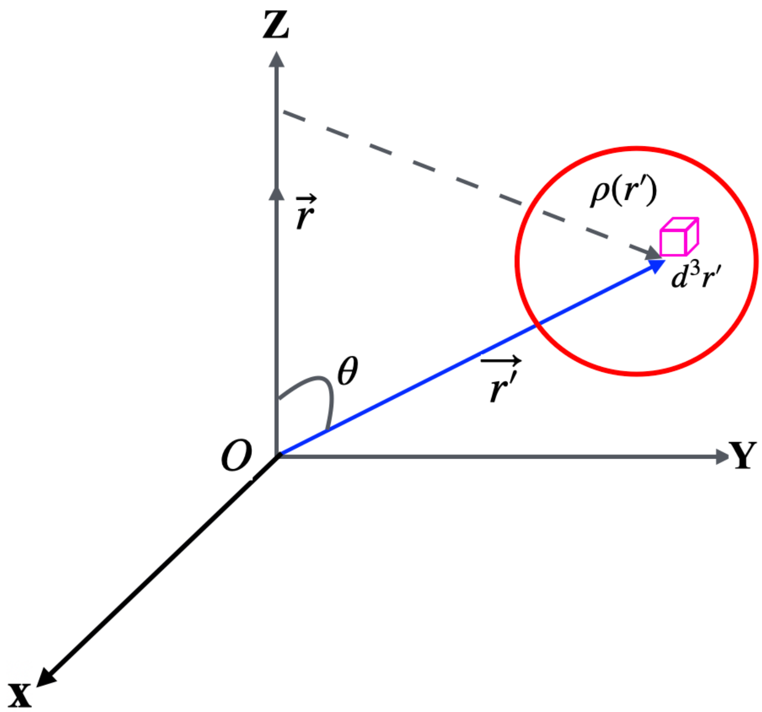

Figure 1.1: Charge distribution $\rho(\boldsymbol{r}')$ inside a nucleus (Fig. 1 of the lecture). An infinitesimal charge element occupies volume d^3r' at $\boldsymbol{r}'$. The field point $\boldsymbol{r}$ lies outside the distribution; θ is the angle between $\boldsymbol{r}$ and $\boldsymbol{r}'$.

The first three polynomials are $P_0 = 1$, $P_1(\cos\theta) = \cos\theta$, and $P_2(\cos\theta) = \frac{1}{2}(3\cos^2\theta - 1)$, so

$$\frac{1}{|\boldsymbol{r}-\boldsymbol{r}'|} = \frac{1}{r}\left(1 + \frac{r'}{r}\cos\theta + \frac{r'^2}{2r^2}(3\cos^2\theta - 1) + \cdots\right). \tag{1.3}$$

The quadrupole term is precisely the $\ell = 2$ piece of this expansion: it is of order $(r'/r)^2$ and must be retained if one wishes to discuss Q. (Omitting r'^2/r^2 would truncate before the quadrupole appears.)

Substitute (1.3) into (1.1):

$$\Phi(\boldsymbol{r}) = \frac{1}{4\pi\varepsilon_0}\int \rho(\boldsymbol{r}')\frac{1}{r}\left(1 + \frac{r'}{r}\cos\theta + \frac{r'^2}{2r^2}(3\cos^2\theta - 1) + \cdots\right)\mathrm{d}^3r'. \tag{1.4}$$

For an axially symmetric source whose symmetry axis is z, collecting powers of $1/r$ gives

$$\Phi(\boldsymbol{r}) = \frac{e}{4\pi\varepsilon_0 r}\left(Z + \frac{D}{r}\,P_1(\cos\theta) + \frac{Q_2}{r^2}\,P_2(\cos\theta) + \cdots\right), \tag{1.5}$$

where

- the **monopole** Z is the total charge (in units of e);
- D is the **electric dipole** moment;
- Q_2 is the Legendre-normalised quadrupole coefficient.

Nuclear ground states of definite parity have vanishing static electric dipole. The first multipole that can report a permanent deformation is therefore the quadrupole.

1.1.3 Definition of the quadrupole tensor

The Cartesian quadrupole tensor associated with the third term of the expansion is

$$Q_{ij} = \int \rho(\boldsymbol{r})\big(3x_i x_j - r^2\delta_{ij}\big)\,\mathrm{d}^3 r, \tag{1.6}$$

with $i, j = x, y, z$ and δ_{ij} the Kronecker symbol. Examples:

$$Q_{xx} = \int \rho(\boldsymbol{r})\,(3x^2 - r^2)\,\mathrm{d}^3 r, \tag{1.7}$$

$$Q_{xy} = \int \rho(\boldsymbol{r})\,(3xy)\,\mathrm{d}^3 r. \tag{1.8}$$

There are nine components, but only five are independent (the tensor is symmetric and traceless). In nuclear spectroscopy the component measured in the stretched state is almost always

$$Q_{\mathrm{spec}} \equiv \frac{Q_{zz}}{e} = \frac{1}{e}\int \rho(\boldsymbol{r})\,(3z^2 - r^2)\,\mathrm{d}^3 r = \langle 3z^2 - r^2\rangle_{\mathrm{charge}}. \tag{1.9}$$

Thus Q_{spec} has units of area and $eQ_{\mathrm{spec}} = Q_{zz}$ has units of charge times area. Nuclear tables quote either Q_{spec} in barns or eQ_{spec} in $e \cdot \mathrm{fm}^2$.

The coefficient in Equation (1.5) is

$$Q_2 = \frac{1}{e}\int \rho(\boldsymbol{r})\,r^2 P_2(\cos\theta)\,\mathrm{d}^3 r = \frac{Q_{zz}}{2e} = \frac{Q_{\mathrm{spec}}}{2}. \tag{1.10}$$

The factor of two follows from $r^2 P_2(\cos\theta) = (3z^2 - r^2)/2$. This convention is used everywhere below: Q_2 belongs in the potential, while quoted nuclear moments are $Q_{\mathrm{spec}} = Q_{zz}/e = 2Q_2$. Classically, $Q_{\mathrm{spec}} > 0$ for a prolate (cigar-like) distribution along z, and $Q_{\mathrm{spec}} < 0$ for an oblate (flattened) one.

1.1.4 Spherical symmetry forces vanishing quadrupole

If the charge density is spherically symmetric, $\rho = \rho(r)$ only, then by symmetry

$$\int z^2 \rho\,\mathrm{d}^3 r = \int x^2 \rho\,\mathrm{d}^3 r = \int y^2 \rho\,\mathrm{d}^3 r = \frac{1}{3}\int r^2 \rho\,\mathrm{d}^3 r. \tag{1.11}$$

Hence $3z^2 - r^2$ averages to zero and

$$Q_{zz} = \int \rho(\boldsymbol{r}')\,(3z^2 - r^2)\,\mathrm{d}^3 r' = 0. \tag{1.12}$$

Equivalently, on a sphere $x^2 = y^2 = z^2$ so $r^2 = 3z^2$ and $3z^2 - r^2 = 0$ pointwise in the average sense of (1.12). **A spherical charge distribution has no electric quadrupole moment.**

1.2 Deuteron quadrupole moment

1.2.1 Pure S-wave implies vanishing Q_d

Free protons and neutrons have vanishing electric quadrupole moments. Any nonzero Q of the deuteron must come from the *orbital* distribution of the proton's charge about the centre of mass.

If the NN potential were purely central, the ground state would be pure $L = 0$. The spatial wave function is then proportional to the spherical harmonic Y_{00}, which is angle-independent. The charge density is therefore spherically symmetric, and the multipole argument of Section 1.1.4 applies at once:

$$Q_d(L{=}0) = 0. \tag{1.13}$$

A pure s-wave deuteron would look electromagnetically spherical.

1.2.2 The measured value

Experiment finds a small but clearly nonzero moment for the bound deuteron [6]:

$$Q_d \equiv Q_{\text{spec}} = \frac{Q_{zz}}{e} = 2.88 \times 10^{-27}\,\text{cm}^2 = 0.00288\,\text{b}, \qquad eQ_d = 0.288\,\text{e}\cdot\text{fm}^2. \tag{1.14}$$

(The unit is area, as required by (1.9); one barn $= 10^{-28}\,\text{m}^2 = 100\,\text{fm}^2$.) The value is tiny compared with collective rare-earth rotors (several barns), but it is not zero. That single experimental fact rules out a pure $L = 0$ ground state and, with it, a purely central NN potential.

A geometric scale eR^2 with $R \sim 2\,\text{fm}$ is a few $e \cdot \text{fm}^2$; the measured $eQ_d \sim 0.3\,e \cdot \text{fm}^2$ is smaller, consistent with a mild deformation from a few-percent D-wave rather than a strongly deformed rotor.

1.2.3 Mixed wave function and the D-state

Using the mixed ground state of Lecture 8,

$$|\psi\rangle = a_S|S\rangle + a_D|D\rangle, \qquad |a_S|^2 + |a_D|^2 = 1,$$

the spectroscopic quadrupole moment in the stretched state is

$$Q_d = \left\langle \psi \left| \frac{\hat{Q}_{zz}}{e} \right| \psi \right\rangle = |a_S|^2 Q_{SS} + 2\,\text{Re}(a_S^* a_D)\,Q_{SD} + |a_D|^2 Q_{DD}. \tag{1.15}$$

The pure-S matrix element vanishes by spherical symmetry, $Q_{SS} = 0$. The interference and pure-D pieces may be written in terms of the radial functions $u(r) = rR_S(r)$ and $w(r) = rR_D(r)$ (standard Blatt–Weisskopf / Reid normalisation) as

$$Q_d = \frac{\sqrt{2}}{10} \int_0^\infty r^2\,(uw - \tfrac{w^2}{\sqrt{8}})\mathrm{d}r \quad \text{(units of area)}, \tag{1.16}$$

with eQ_d quoted in $e \cdot \mathrm{fm}^2$. Equivalently, the dominant contribution is the S–D interference term $\propto a_S a_D$; the pure D–D piece is smaller because P_D itself is small. Evaluating the radial integrals requires a model for $u(r)$ and $w(r)$. Realistic potentials fitted to NN scattering reproduce $Q_d \approx 0.286\,\mathrm{fm}^2$ with a few-percent D-state probability, consistent with the magnetic-moment estimate of Lecture 8 once exchange currents are acknowledged [6]. The positive sign of Q_d means a prolate (cigar-like) charge distribution along the spin axis.

Key idea

Two multipoles, one structure.

Observable	Pure S prediction	Experiment
μ_d/μ_N	0.880	0.857
Q_d	0	$0.00288\,\mathrm{b}$

Both point to a small D-wave. The quadrupole moment is an on/off signal of nonsphericity; the magnetic moment is a percent-level correction to an already large spin moment.

Caution

Extracting P_D from Q_d alone is model dependent because the D-state radial wave function is not measured directly. Potentials that produce a few-percent D-state also produce the observed Q_d, and scattering analyses agree. The qualitative need for a tensor force does not rest on a single fitted percentage [6].

1.3 Non-central force and the tensor operator

1.3.1 Why a central potential cannot mix L

In a purely central potential $V(r)$, orbital angular momentum is a constant of the motion: $[\boldsymbol{L}^2, H] = 0$. Energy eigenstates may therefore be chosen with definite L. A single eigenstate cannot be a coherent superposition of $L = 0$ and $L = 2$. Experiment, however, requires precisely that mixture: $Q_d \neq 0$ and the magnetic-moment deficit. The residual NN interaction therefore cannot be purely central; it must contain a piece that does not commute with $\boldsymbol{L}^2$.

Spin–spin forces of the form $V_\sigma(r)\,\boldsymbol{\sigma}_1 \cdot \boldsymbol{\sigma}_2$ still depend only on the relative distance: they split triplet from singlet but do not mix different L. The operator that couples S and D must involve the orientation of the relative vector $\boldsymbol{r}$ with respect to the nucleon spins.

1.3.2 Magnetic-dipole analogy and the tensor operator

A familiar non-central interaction is the force between two magnetic dipoles. At fixed separation the energy depends on how the moments are oriented relative to $\hat{\boldsymbol{r}}$: collinear and sideways arrangements are not equivalent.

Classically,

$$U \propto \frac{3(\boldsymbol{m}_1 \cdot \hat{r})(\boldsymbol{m}_2 \cdot \hat{r}) - \boldsymbol{m}_1 \cdot \boldsymbol{m}_2}{r^3}.$$

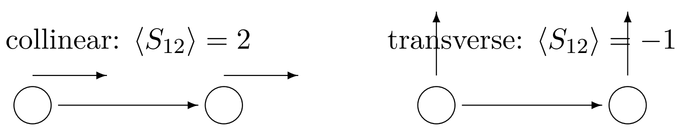

same separation r, different tensor energy

$$S_{12} = 3(\boldsymbol{\sigma}_1\cdot\hat{r})(\boldsymbol{\sigma}_2\cdot\hat{r}) - \boldsymbol{\sigma}_1\cdot\boldsymbol{\sigma}_2$$

Figure 1.2: Two dipoles at fixed r: collinear versus tilted. The force depends on orientation, so it is non-central.

Replacing magnetic moments by nucleon spin operators yields the **tensor operator**

$$S_{12} = 3(\boldsymbol{\sigma}_1 \cdot \hat{r})(\boldsymbol{\sigma}_2 \cdot \hat{r}) - \boldsymbol{\sigma}_1 \cdot \boldsymbol{\sigma}_2, \tag{1.17}$$

and a potential piece $V_T(r)\, S_{12}$. In the coupled ${}^3S_1$–${}^3D_1$ subspace the angular matrix elements of S_{12} are standard:

$$\langle {}^3S_1|S_{12}|{}^3S_1\rangle = 0, \quad \langle {}^3S_1|S_{12}|{}^3D_1\rangle = \sqrt{8}, \quad \langle {}^3D_1|S_{12}|{}^3D_1\rangle = -2. \tag{1.18}$$

(For a spin-triplet product state polarised along an axis making angle ϑ with $\hat{r}$, $\langle S_{12}\rangle = 3\cos^2\vartheta - 1$: it is $+2$ for spins parallel to the separation and -1 for spins transverse to it. The interaction is therefore orientation dependent even at fixed r.)

The selection rule also follows from the operator structure: S_{12} is the scalar coupling of a rank-2 spherical harmonic $Y_2(\hat{r})$ to a rank-2 spin tensor. The orbital matrix element obeys

$$|L - L'| \le 2 \le L + L', \qquad (-1)^{L'} = (-1)^L,$$

so it connects $\Delta L = 0, \pm 2$ while conserving total J and parity. Starting from $L = 0$, the anisotropic part can therefore connect only $L' = 2$. This is the ${}^3S_1 \leftrightarrow {}^3D_1$ selection rule; the S-wave diagonal angular average vanishes. (The vanishing S–S diagonal shows that a pure central spin–spin force cannot mix L; only the off-diagonal tensor matrix element does.) Writing the radial wave as $\psi = u(r)Y_S + w(r)Y_D$, the coupled radial Schrödinger equations in the deuteron channel become

$$-\frac{\hbar^2}{m}\frac{\mathrm{d}^2u}{\mathrm{d}r^2} + V_C u + \sqrt{8}\, V_T w = Eu, \tag{1.19}$$

$$-\frac{\hbar^2}{m}\left(\frac{\mathrm{d}^2w}{\mathrm{d}r^2} - \frac{6w}{r^2}\right) + (V_C - 2V_T - 3V_{LS})w + \sqrt{8}\, V_T u = Ew, \tag{1.20}$$

where V_C collects central (including spin–spin) pieces and V_{LS} is the spin–orbit term. The off-diagonal $\sqrt{8}\, V_T$ is precisely what mixes u and w and generates $Q_d \neq 0$.

One-pion exchange produces exactly this tensor structure at long range, with radial factors $e^{-m_\pi r}/r$ and polynomials in $1/(m_\pi r)$ [6, 2, 4, 9]. In the deuteron channel V_T mixes ${}^3S_1$ with ${}^3D_1$, generates $Q_d \neq 0$, and shifts μ_d by a few percent. That mixing is the clearest bound-state evidence for the tensor character of the residual nuclear force [6].

Definition

Tensor force. The non-central NN potential contains $V_T(r)S_{12}$. In the deuteron it is responsible for S–D mixing, for $Q_d \neq 0$, and for the small correction to μ_d.

1.3.3 The full NN potential is richer

Phenomenological potentials include central, spin–spin, tensor, spin–orbit, and short-range terms, with isospin dependence. The deuteron bound state has taught us the first three. Scattering (all partial waves, both singlet and triplet, as functions of energy) fixes the rest. When the bound state runs out of information, the continuum (scattering) takes over.

1.4 Quadrupole moments of heavier nuclei (context)

Tables of quadrupole moments place the deuteron in perspective. Many nuclei have $|Q|$ of order eR^2 (single-particle scale). Rare-earth nuclei reach several barns: the whole proton distribution is collectively deformed. Closed-shell nuclei have $Q \approx 0$. For deformed heavy nuclei one distinguishes the **intrinsic** quadrupole moment Q_0 in the body-fixed frame from the **spectroscopic** moment measured in the laboratory; they differ by a projection factor depending on I. The deuteron is the few-body extreme: weak binding, small spectroscopic Q, tensor-driven rather than collective [6, 1].

1.5 Synthesis: Lectures 7–9

Lecture	Observable	Lesson
7	$B_d \approx 2.224\,\mathrm{MeV}$	Range $\sim 2\,\mathrm{fm}$, depth $\sim 35\,\mathrm{MeV}$; barely bound
8	$I^\pi = 1^+$, $\mu_d = 0.857\,\mu_N$	Triplet; $\sim 96\%\ S + \sim 4\%\ D$; spin-dependent force
9	$Q_d = 0.00288\,\mathrm{b}$	Nonspherical; tensor force $V_T S_{12}$

Takeaway

Physics of Lecture 9.

- $Q_{\text{spec}} = Q_{zz}/e = \langle 3z^2 - r^2\rangle_{\text{charge}}$: vanishes for spherical charge distributions.
- $Q_d = 0.00288\,\mathrm{b} \neq 0$: the deuteron is not a pure S-state.
- Consistent few-percent D-wave from μ_d and Q_d.
- Tensor operator S_{12} encodes the non-central force; pion exchange is its long-range origin.
- Lectures 7–9 define the qualitative NN force; Lectures 10–11 develop scattering phase shifts and meson exchange for the course.

1.6 Deeper physics: spectroscopic Q, shells, and one-pion tensor force

1.6.1 Intrinsic vs spectroscopic quadrupole moment

For deformed heavy nuclei one distinguishes the **intrinsic** quadrupole moment Q_0 in the body-fixed frame from the **spectroscopic** moment Q measured in the lab. They are related by a Clebsch–Gordan projection factor depending on I. For the deuteron $I = 1$ there is no collective rotor picture: Q_d is a few-body matrix element of $r^2 Y_{20}$ between S and D components. Standard values are

$$Q_d \approx +0.286\,\mathrm{fm}^2, \qquad eQ_d \approx +0.286\,\mathrm{e}\cdot\mathrm{fm}^2 \tag{1.21}$$

and stresses that free nucleons have $Q = 0$, so any nonzero deuteron Q is purely orbital / deformation physics [6].

1.6.2 Shell-model systematics of Q

The plot of quadrupole moments versus Z shows sign changes near magic numbers: closed shells are spherical ($Q \approx 0$); a valence proton hole just below a shell tends to give prolate $Q > 0$, while a particle just above tends toward oblate $Q < 0$ in the single-particle picture. Collective mid-shell nuclei have Q many times the single-particle estimate. The deuteron sits at the opposite extreme: no shells, weak binding, small Q generated by tensor-driven D-wave admixture [1].

1.6.3 One-pion exchange and S_{12}

The long-range NN force is one-pion exchange (Yukawa). The pseudoscalar pion coupling produces a potential containing the tensor operator S_{12} with radial dependence

$$V_T(r) \propto \frac{e^{-m_\pi r}}{r}\left(1 + \frac{3}{m_\pi r} + \frac{3}{(m_\pi r)^2}\right) \tag{1.22}$$

(up to spin–isospin factors). The angular matrix elements (1.18) then feed into the coupled equations (1.19)–(1.20), so pion exchange is the microscopic origin of the magnetic-dipole analogy in the lecture: it is non-central and mixes ${}^3S_1$–${}^3D_1$. Short-range repulsion, spin–orbit forces, and multi-pion / contact terms complete modern potentials (Argonne, CD-Bonn, chiral EFT). The deuteron Q_d and η_D (D/S asymptotic ratio) are primary constraints on V_T [6, 4, 2].

Key idea

Tensor force checklist.

- Operator: $S_{12} = 3(\boldsymbol{\sigma}_1 \cdot \hat{r})(\boldsymbol{\sigma}_2 \cdot \hat{r}) - \boldsymbol{\sigma}_1 \cdot \boldsymbol{\sigma}_2$.
- Bound-state signals: $Q_d \neq 0$, $\mu_d \neq \mu_p + \mu_n$, few-percent D-state probability (model dependent).
- Continuum signals: mixing parameters in NN phase-shift analyses (ε_1, etc.).
- Microscopic origin: one-pion exchange at long range.

1.6.4 What remains for scattering

Bound-state multipoles fix the deuteron channel. Scattering states access all partial waves, both singlet and triplet, as functions of energy. Phase shifts $\delta_{^1S_0}(E)$, $\delta_{^3S_1}(E)$, P- and D-wave phase shifts, and mixing angles complete the NN interaction and feed into many-body nuclear structure. That programme is the natural continuation of Lectures 7–9 [2, 6].

1.7 Quadrupole moment and the tensor operator

1.7.1 Why $Q_d \neq 0$ requires S–D interference

A pure $^3S_1$ state has spherical symmetry and $Q_d = 0$. The measured $Q_d = +0.286\,\mathrm{fm}^2$ therefore proves an admixture of $L = 2$. In the coupled S–D basis the quadrupole operator $Q \propto r^2 Y_{20}$ has non-zero matrix elements between $L = 0$ and $L = 2$, so the expectation value scales as

$$Q_d \propto a_S a_D \,\langle r^2\rangle_{SD} + a_D^2 \,\langle r^2\rangle_{DD}, \tag{1.23}$$

with amplitudes a_S and a_D. The linear $a_S a_D$ term dominates when $a_D \ll 1$: Q_d is sensitive to the *phase* of the D-wave as well as its magnitude. The positive sign corresponds to prolate deformation (charge extended along the spin quantisation axis).

1.7.2 Angular structure of S_{12}

The tensor operator

$$S_{12} = 3(\boldsymbol{\sigma}_1 \cdot \hat{r})(\boldsymbol{\sigma}_2 \cdot \hat{r}) - \boldsymbol{\sigma}_1 \cdot \boldsymbol{\sigma}_2 \tag{1.24}$$

couples spin to the separation vector. For nucleon spins aligned along $\hat{z}$, a short calculation gives $S_{12} = +2$; for spins perpendicular to $\hat{r}$ in the equatorial plane, $S_{12} = -1$. A central force averaged over a spherical s-wave vanishes on S_{12}, but the $^3S_1$–$^3D_1$ coupling does not. One-pion exchange generates (1.24) with Yukawa range $r_0 = \hbar/(m_\pi c)$ (Lecture 11), providing the microscopic link between pion physics and deuteron deformation.

Order-of-magnitude Q_d

With $r_{\mathrm{rms}} \approx 2.1\,\mathrm{fm}$, a classical estimate $Q \sim er^2 \sim 0.4\,\mathrm{e}\cdot\mathrm{fm}^2$ sets the scale. The measured $eQ_d \approx 0.29\,\mathrm{e}\cdot\mathrm{fm}^2$ is smaller because only the few-percent D-wave contributes coherently. Requiring (1.23) to match experiment with $a_D^2 \sim 0.05$ is consistent with the P_D inferred from μ_d in Lecture 8.

Remark

Continuum counterpart. Bound-state $\eta_D = a_D/a_S$ at large r is mirrored in NN scattering by the $^3S_1$–$^3D_1$ mixing parameter $\varepsilon_1(E)$ (Lecture 10). Potentials tuned to B_d, μ_d, and Q_d must simultaneously reproduce low-energy triplet phase shifts; failure in any one channel signals missing physics (three-body forces, relativistic effects, or inconsistent currents).

1.7.3 Electrostatic multipole expansion at $A = 2$

Outside the charge distribution the deuteron potential admits

$$\Phi(r,\theta) = \frac{e}{r} + \frac{1}{4\pi\varepsilon_0}\frac{1}{2r^3}\sum_{m=-2}^{2} Q_{2m}\, Y_{2m}(\theta,\phi) + \cdots \tag{1.25}$$

The monopole is the proton charge (neutron uncharged); the dipole vanishes for parity reasons; the quadrupole is the first deformation signal. Because $Q_d \propto a_S a_D$, measuring Q_d fixes the *product* of S and D amplitudes, while μ_d (Lecture 8) constrains their relative phase and spin content. No single deuteron observable alone yields $P_D = a_D^2$; the trio (B_d, μ_d, Q_d) is the minimal static set [6, 14].

1.7.4 Tensor force in heavier nuclei (preview)

The same S_{12} operator that mixes ${}^3S_1$ and ${}^3D_1$ in the deuteron contributes to spin–orbit splittings in the mean field (Lecture 12) and to the alignment of high-momentum pairs in short-range correlation studies. At $A = 2$ the tensor expectation is a few percent; in $A \sim 50$ nuclei it can drive shell reordering when combined with deformation (Lecture 15). The deuteron is the cleanest place to learn the operator before it is masked by many-body averaging [1, 4].

1.8 Further physics: multipoles beyond the quadrupole

Outside a localised charge distribution the electrostatic potential admits a multipole expansion: monopole (total charge), dipole (vanishes for definite-parity ground states), quadrupole, octupole, … At large distance the lowest non-vanishing multipole dominates [13, 1, 6].

The same logic applies to magnetic multipoles and to radiation. In γ decay, multipole selection rules (angular momentum and parity of the photon field) organise transition rates (a topic for later lectures). For the deuteron ground state the essential static multipoles are already in hand: magnetic dipole μ_d and electric quadrupole Q_d. Together they require a tensor force and a few-percent D-wave, completing the qualitative NN picture of Lectures 7–9.

1.8.1 Deformation and quadrupole moments of heavier nuclei

Nuclei near closed (magic) shells are nearly spherical and have small Q. Nuclei far from magic numbers are often permanently deformed and can have large spectroscopic quadrupole moments; rotational bands appear in the spectrum [14, 6, 13]. The deuteron is the opposite extreme: few-body, weakly deformed, with Q_d generated by a small D-wave rather than collective rotation.

Static multipoles (monopole, dipole, quadrupole, …) also organise electromagnetic radiation: γ transitions carry multipolarity $E1, M1, E2, \ldots$ with selection rules fixed by angular momentum and parity [13], the dynamical counterpart of the static moments used here.

1.8.2 Deuteron quadrupole moment in numbers

The free neutron and proton have vanishing electric quadrupole moments, so any $Q_d \neq 0$ must come from orbital structure. Experiment gives

$$Q_d = +0.00288\,\mathrm{b} = +0.286\,\mathrm{fm}^2, \tag{1.26}$$

small compared with heavy deformed nuclei but definitely nonzero [6]. A pure ${}^3S_1$ wave function would yield $Q_d = 0$. A mixed $S+D$ wave function produces

$$Q_d \propto a_S a_D \,\langle r^2 \rangle_{SD} + a_D^2 \,\langle r^2 \rangle_{DD}, \tag{1.27}$$

so Q_d is linearly sensitive to the S–D interference. Realistic potentials that fit scattering and B_d reproduce Q_d with a_D^2 of a few percent, consistent with the magnetic-moment estimate [6, 14].

The positive sign of Q_d corresponds to a prolate (cigar-like) deformation: more charge along the symmetry axis than in the equatorial plane.

1.8.3 Single-particle vs collective quadrupole moments

For a single valence proton in an orbit of mean-square radius $\langle r^2 \rangle \sim R^2 \sim r_0^2 A^{2/3}$, one expects

$$|Q| \lesssim e\,R^2 \sim 0.06\text{–}0.5\,e \cdot \mathrm{b} \tag{1.28}$$

from light to heavy nuclei. Many odd-A moments fall in that range, but rare-earth and actinide nuclei reach several $e \cdot \mathrm{b}$: the entire charged core is permanently deformed, so many protons contribute coherently [6, 2]. Even–even nuclei have vanishing spectroscopic Q in the laboratory frame if $I = 0$, but large *intrinsic* quadrupole moments show up in rotational spectra and in Coulomb excitation.

1.8.4 Tensor operator S_{12} and noncentral force

The simplest scalar operator that couples spin and relative coordinate is

$$S_{12} = 3(\boldsymbol{\sigma}_1 \cdot \hat{\boldsymbol{r}})(\boldsymbol{\sigma}_2 \cdot \hat{\boldsymbol{r}}) - \boldsymbol{\sigma}_1 \cdot \boldsymbol{\sigma}_2. \tag{1.29}$$

A potential $V_T(r)\,S_{12}$ is the tensor force. It vanishes when averaged over a spherically symmetric s-wave alone, but it mixes ${}^3S_1$ and ${}^3D_1$ and generates Q_d. In heavier nuclei the same tensor force contributes to the spin-orbit splitting and to few-nucleon binding, though its expectation value is partially averaged by many-body motion [14, 6].

One-pion exchange naturally produces a tensor potential of Yukawa range $r_0 \approx 1.4\,\mathrm{fm}$; that is the long-range reason the deuteron is not a pure s-wave state [9, 14].

1.8.5 Parity and multipole selection

A static electric multipole of order ℓ has parity $(-1)^\ell$; a magnetic multipole has parity $(-1)^{\ell+1}$. Nuclear ground states of definite parity therefore forbid static electric dipoles: the lowest allowed electric deformation is the quadrupole. That is why Q is the first multipole beyond the monopole in the structural discussion of the deuteron and of deformed heavy nuclei [1, 6].

1.8.6 Evaluating S_{12} in the S–D basis

For two spin-$\frac{1}{2}$ particles with $\boldsymbol{S} = \boldsymbol{s}_1 + \boldsymbol{s}_2$, the tensor operator (1.24) has non-zero matrix elements only between states of the same total S and differing L by $\Delta L = 2$. In the ${}^3S_1$–${}^3D_1$ coupled channel, the off-diagonal element $\langle D|S_{12}|S\rangle$ is proportional to $\langle 2, 0; 1, 0|1, 0\rangle$ Clebsch–Gordan factors and sets the mixing rate. A radial integral over $V_T(r)\, u_S(r)\, u_D(r)$ converts the operator into an energy shift and a level coupling. One-pion exchange supplies $V_T(r) \propto e^{-m_\pi r}/r^3$ at long range (Lecture 11), so the D-wave admixture is tied directly to pion physics rather than to an arbitrary off-diagonal potential.

1.8.7 Consistency of μ_d, Q_d, and η_D

Modern NN fits require simultaneous agreement with:

1. B_d (Lecture 7 square-well threshold);
2. μ_d (Lecture 8 magnetic moment);
3. Q_d and η_D (this lecture);
4. triplet s-wave scattering length a_t (Lecture 10).

A potential that fits B_d but misses Q_d typically has incorrect tensor strength; one that fits Q_d but misses μ_d may have right tensor geometry but wrong current operators. The deuteron is therefore a *constraint bundle*, not a single-number benchmark.

Classical quadrupole vs experiment

A uniform charge distribution in a prolate spheroid with semi-axis $a = 2.0\,\mathrm{fm}$ and $b = 1.5\,\mathrm{fm}$ has $Q \sim \frac{2}{5}e(a^2 - b^2) \approx 0.5\,\mathrm{e}\cdot\mathrm{fm}^2$. The measured $eQ_d \approx 0.29\,\mathrm{e}\cdot\mathrm{fm}^2$ is smaller because only the D-wave fraction ($\sim 5\%$) contributes. Dividing the experimental value by the classical estimate gives a rough $a_D^2 \sim 0.06$, consistent with the P_D from Lecture 8.

1.8.8 Bridge to shell-model Q systematics

Heavy-nucleus quadrupole moments (Section 1.6.2) arise from collective deformation or valence-shell orbits, not from S–D mixing. The tensor force that shapes the deuteron reappears in the nuclear mean field as spin–orbit and deformation-driving terms (Lectures 12–13). The sign changes of Q near magic numbers and the large Q of rare-earth nuclei (Lecture 15) are many-body amplifications of the same operator structure seen at $A = 2$ [6, 1].

1.8.9 Asymptotic D/S ratio η_D

At large r the S and D components behave as $u_S \sim e^{-\gamma r}$ and $u_D \sim \eta_D e^{-\gamma r}$ with the same γ (Lecture 7). Electron scattering and tensor-polarisation observables constrain η_D independently of the interior potential. Because $Q_d \propto a_S a_D$ and μ_d depends on the same product with different angular weighting, (Q_d, η_D, μ_d) overconstrain fits if the current operator is held fixed. Modern analyses treat η_D as a standard deuteron observable alongside B_d and r_{rms} [6, 14].

1.9 Deeper reading: Q_d, S_{12}, and high-momentum pairs

Without the tensor operator S_{12}, a pure S-wave deuteron has vanishing quadrupole moment. The measured $Q_d > 0$ is therefore direct evidence for tensor-driven S–D mixing. One-pion exchange supplies the long-range tensor force; short-range cutoffs regulate the contact pieces. In many-body systems the same tensor correlations produce high-momentum neutron–proton pairs observed as short-range correlations and drive shell evolution away from stability (Lecture 12).

A classical estimate $Q \sim r^2$ with $r \sim 2\,\text{fm}$ gives the correct mega-femtometre-squared scale, but the quantum matrix element depends on the relative phase of S and D waves. When reading SRC ratios, keep them distinct from mean-field single-particle energy shifts: both are tensor-related, yet they probe different momentum domains. Lectures 10–11 then embed this force piece into scattering and meson exchange more broadly.

Operator identities and expectation values

Evaluate S_{12} for spin-aligned and spin-antialigned configurations to recover the classic factors $+2$ and -1. Those factors explain why the tensor force is attractive in the deuteron channel and repulsive in others. In momentum space, the tensor force mixes high relative momenta, feeding the SRC plateau observed in exclusive electron scattering.

Shell-evolution sketch

A schematic tensor force shifts single-particle energies of $j_>$ and $j_<$ partners differently as protons or neutrons fill spin–orbit partners. That differential shift is a leading explanation for magic-number migration (Lecture 12). Classroom discussions should separate this mean-field tensor effect from high-momentum SRC fractions: same operator family, different probes.

Tensor force across scales

At long distance, one-pion exchange generates a tensor potential $\propto S_{12}(e^{-m_\pi r}/r)$ times a radial function. At short distance, contacts and heavier-meson exchanges cut off the singularity. The deuteron D-wave lives primarily in the intermediate region where one-pion exchange is trustworthy, which is why Q_d is a relatively clean tensor observable compared with high-momentum SRC ratios.

In a nucleus, the same operator has a mean-field avatar (single-particle energy shifts) and a short-range avatar (high-momentum pairs). A student literature note should cite one example of each and refuse to conflate their percentages. Bridging to Lecture 12, sketch how filling a $j_>$ proton orbital shifts neutron $j_<$ energies via the tensor force: that cartoon is sufficient preparation for modern shell-evolution discussions without requiring a full G-matrix derivation.

The tensor force is the structural thread from Q_d to shell evolution and SRC. Keeping long-distance and short-distance tensor manifestations separate is essential for clear reasoning.

In practice, rework one numerical estimate from the lecture with a different parameter set and compare the shift to the quoted experimental uncertainty. If the shift exceeds the uncertainty, the estimate is teaching a scale, not delivering a fit. That distinction keeps theoretical cartoons honest when they sit beside evaluated data tables and modern many-body calculations. Along the course arc, write one sentence linking this chapter backward and one forward: the discipline of those two sentences is as important as any single formula. Examination problems rarely ask for a literature review, but they do ask for the scale argument that literature reviews presuppose.

Research frontier: tensor force, SRC, and student projects

The deuteron quadrupole moment of Lecture 9 is the cleanest static signature of the tensor force: without S_{12}, a pure S-wave deuteron would have $Q_d = 0$. In many-body systems the same tensor component drives shell evolution in exotic nuclei (migration of single-particle energies and islands of inversion) and correlates high-momentum nucleon–nucleon pairs observed as short-range correlations (SRC) in exclusive electron scattering [43, 41]. Chiral EFT organises the tensor force from one-pion exchange upward, while SRC studies connect laboratory high-momentum fractions to the dense-matter equation of state and to the neutron-proton dominance of correlated pairs [42]. Open questions include the quantitative link between measured SRC ratios and the high-density symmetry energy, and how much of shell evolution is tensor-driven versus continuum- or central-force-driven in specific isotopic chains.

Experimentally, SRC studies use exclusive $(e, e'pN)$ reactions to isolate high-relative-momentum pairs, while structure studies infer tensor-driven shell evolution from energy gaps and spectroscopic factors. A student literature survey that keeps those two communities' observables distinct avoids mixing correlation fractions with mean-field single-particle shifts. Keeping SRC ratios and mean-field shell gaps as distinct observables prevents double counting when students survey the tensor-force literature.

Student directions. (1) Analytic exercise: evaluate S_{12} for aligned and perpendicular spin orientations and recover the lecture factors $+2$ and -1. (2) Scale estimate: estimate the classical quadrupole scale $Q \sim r^2$ for $r \sim 2\,\text{fm}$ and compare with Q_d. (3) Literature note: summarise one experimental SRC ratio (e.g. np dominance) and its implication for neutron-rich matter.

1.10 Problems with solutions

Problem 9.1 — $Q = 0$ for a sphere

Show that $Q_{zz} = \int \rho(3z^2 - r^2)\,\mathrm{d}^3r$ vanishes for any spherically symmetric $\rho(r)$.

Solution 9.1

Spherical symmetry $\Rightarrow \int x^2\rho = \int y^2\rho = \int z^2\rho = \frac{1}{3}\int r^2\rho$. Hence

$$\int (3z^2 - r^2)\rho = 3 \cdot \tfrac{1}{3}\int r^2\rho - \int r^2\rho = 0.$$

A pure $L = 0$ deuteron would have $Q_d = 0$ [6].

Problem 9.2 — Units of Q_d

The deuteron quadrupole moment is $Q_d = 0.00288\,\mathrm{b}$ and also $2.88 \times 10^{-27}\,\mathrm{cm}^2$. Convert the barn value to $\mathrm{e} \cdot \mathrm{fm}^2$ ($1\,\mathrm{b} = 100\,\mathrm{fm}^2$) and verify consistency with $10^{-27}\,\mathrm{cm}^2$.

Solution 9.2

$$0.00288\,\mathrm{b} = 0.00288 \times 100 = 0.288\,\mathrm{fm}^2, \qquad eQ_d = 0.288\,\mathrm{e} \cdot \mathrm{fm}^2$$

(the first is $Q_d = Q_{zz}/e$; the second restores the charge unit). Also $1\,\mathrm{b} = 10^{-28}\,\mathrm{m}^2 = 10^{-24}\,\mathrm{cm}^2$, so

$$0.00288\,\mathrm{b} = 0.00288 \times 10^{-24}\,\mathrm{cm}^2 = 2.88 \times 10^{-27}\,\mathrm{cm}^2,$$

matching the lecture value. Compared with eR^2 for $R \sim 2\,\mathrm{fm}$ ($\sim 4\,e \cdot \mathrm{fm}^2$), the deformation is mild [6].

Problem 9.3 — Valid far-field expansion and the factor of two

Starting from the exact identity

$$\frac{1}{|\boldsymbol{r} - \boldsymbol{r}'|} = \frac{1}{r}\left(1 - 2\epsilon\cos\theta + \epsilon^2\right)^{-1/2} \qquad \left(\epsilon \equiv \frac{r'}{r} < 1\right),$$

expand through $O(\epsilon^2)$. For an axial charge distribution show that the potential coefficient $Q_2 = e^{-1}\int \rho r'^2 P_2(\cos\theta')\,\mathrm{d}^3r'$ satisfies $Q_2 = Q_{zz}/(2e) = Q_{\mathrm{spec}}/2$.

Solution 9.3

Put $x = -2\epsilon\cos\theta + \epsilon^2$ in $(1+x)^{-1/2} = 1 - \frac{1}{2}x + \frac{3}{8}x^2 + \cdots$. Keeping all terms through ϵ^2,

$$\frac{1}{|\boldsymbol{r} - \boldsymbol{r}'|} = \frac{1}{r}\left[1 + \epsilon\cos\theta + \frac{\epsilon^2}{2}(3\cos^2\theta - 1) + \cdots\right]$$

The ϵ^2 term is exactly $(r'^2/r^2)P_2(\cos\theta)$. Along the symmetry axis,

$$eQ_2 = \int \rho r'^2 P_2(\cos\theta')\,\mathrm{d}^3r' = \frac{1}{2}\int \rho(3z'^2 - r'^2)\,\mathrm{d}^3r' = \frac{1}{2}Q_{zz}.$$

Hence $Q_2 = Q_{\mathrm{spec}}/2$, which is the required convention check [6, 1].

Problem 9.4 — Why a tensor force is required

Given $I^\pi = 1^+$, $\mu_d \neq \mu_p + \mu_n$, and $Q_d \neq 0$, explain why a purely central NN potential is ruled out.

Solution 9.4

A central potential conserves L, so each energy eigenstate has definite L. Even parity and $I = 1$ allow $L = 0$ and $L = 2$ separately, but not a coherent mixture in one eigenstate. Nonzero Q_d requires nonsphericity (D-wave), and the μ_d deficit requires the same mixture. The tensor force $V_T(r)S_{12}$ is the non-central operator that mixes ${}^3S_1$ and ${}^3D_1$ [6, 14].

Problem 9.5 — Tensor operator on a pure S-wave

The tensor operator is $S_{12} = 3(\boldsymbol{\sigma}_1 \cdot \hat{r})(\boldsymbol{\sigma}_2 \cdot \hat{r}) - \boldsymbol{\sigma}_1 \cdot \boldsymbol{\sigma}_2$. Argue why $\langle S_{12}\rangle = 0$ in a pure ${}^3S_1$ state with spherical average, yet S_{12} can still mix S and D waves.

Solution 9.5

In a pure s-wave the orbital density is isotropic. Averaging $(\boldsymbol{\sigma}_1 \cdot \hat{r})(\boldsymbol{\sigma}_2 \cdot \hat{r})$ over angles reduces it to $\frac{1}{3}\boldsymbol{\sigma}_1 \cdot \boldsymbol{\sigma}_2$, so $\langle S_{12}\rangle = 0$. Off-diagonal matrix elements between $L = 0$ and $L = 2$ need not vanish: S_{12} transforms as a rank-2 tensor and connects $\Delta L = 2$. That is how a small D-wave is generated even though the pure-S diagonal expectation is zero [14, 6].

Problem 9.6 — Geometric scale of Q

Estimate the single-particle quadrupole scale eR^2 for $R = r_0 A^{1/3}$ with $r_0 = 1.2\,\text{fm}$ at $A = 2$ and at $A = 160$. Compare with $Q_d = 0.288\,e \cdot \text{fm}^2$ and with rare-earth moments of several $e \cdot \text{b}$.

Solution 9.6

$$R(A{=}2) \approx 1.2 \times 1.26 \approx 1.5\,\text{fm}, \quad eR^2 \approx 2.3\,e \cdot \text{fm}^2;$$

$$R(A{=}160) \approx 1.2 \times 5.4 \approx 6.5\,\text{fm}, \quad eR^2 \approx 42\,e \cdot \text{fm}^2 = 0.42\,e \cdot \text{b}.$$

Q_d is $\ll eR^2(A{=}2)$ (weak D-wave deformation). Collective rare-earth $Q \sim$ few b exceed the single-particle scale by an order of magnitude (coherent core deformation) [6, 2].

Problem 9.7 — Tensor orientation and selection rule

For a triplet product state with both spins polarised along z, evaluate $\langle S_{12}\rangle$ when $\hat{r} \parallel \hat{z}$ and when $\hat{r} \perp \hat{z}$. Then use the rank and parity of S_{12} to explain why it couples $L = 0$ to $L = 2$, but not to $L = 1$.

Solution 9.7

For the aligned triplet, $\langle \boldsymbol{\sigma}_1 \cdot \boldsymbol{\sigma}_2\rangle = 1$. If $\hat{r} \parallel \hat{z}$, each projected Pauli operator has eigenvalue $+1$, so $\langle S_{12}\rangle = 3 - 1 = 2$. If $\hat{r} \perp \hat{z}$, each one-spin transverse expectation vanishes, so $\langle S_{12}\rangle = -1$. The interaction is orientation dependent.

The orbital part is rank 2 and even under parity. The triangle rule permits $|L - L'| \le 2 \le L + L'$, while parity requires L and L' to have the same parity. From $L = 0$, only $L' = 2$

survives; $L' = 1$ has the wrong parity. Thus the tensor force produces the observed S–D mixing.

Bibliography

[1] R. A. Dunlap, *An Introduction to the Physics of Nuclei and Particles* (2nd ed.), IOP Publishing, Bristol (2023), DOI: 10.1088/978-0-7503-6094-4, Ch. 3 (Nuclear composition and size).

[2] W. Demtröder, *Nuclear and Particle Physics*, Undergraduate Lecture Notes in Physics, Springer, Cham (2023).

[3] S. Petrera, *Problems and Solutions in Nuclear and Particle Physics*, UNITEXT for Physics, Springer, Cham (2019).

[4] F. Terranova, *A Modern Primer in Particle and Nuclear Physics*, Oxford University Press (2021).

[5] S. D'Auria, *Introduction to Nuclear and Particle Physics*, Undergraduate Lecture Notes in Physics, Springer, Cham (2018).

[6] K. S. Krane, *Introductory Nuclear Physics*, Wiley, New York (1988).

[7] R. Hofstadter, "Electron scattering and nuclear structure," Rev. Mod. Phys. **28**, 214 (1956).

[8] H. F. Ehrenberg, R. Hofstadter, U. Meyer-Berkhout, D. G. Ravenhall, and S. E. Sobottka, "High-Energy Electron Scattering and the Charge Distribution of Carbon-12 and Oxygen-16," Phys. Rev. **113**, 666 (1959).

[9] H. Yukawa, "On the interaction of elementary particles. I," Proc. Phys.-Math. Soc. Japan **17**, 48 (1935).

[10] R. D. Woods and D. S. Saxon, "Diffuse surface optical model for nucleon-nuclei scattering," Phys. Rev. **95**, 577 (1954).

[11] H. G. J. Moseley, "The high-frequency spectra of the elements," Phil. Mag. **26**, 1024 (1913); **27**, 703 (1914).

[12] C. F. von Weizsäcker, "Zur Theorie der Kernmassen," Z. Phys. **96**, 431 (1935).

[13] P. Cappellaro, *Introduction to Applied Nuclear Physics* (MIT OpenCourseWare / LibreTexts), CC BY-NC-SA 4.0.

[14] J.-L. Basdevant, J. Rich, and M. Spiro, *Fundamentals in Nuclear Physics: From Nuclear Structure to Cosmology*, Springer, New York (2005).

[15] D. Tong, *Particle Physics*, Lecture notes (University of Cambridge / CERN school notes).

[16] M. G. Mayer, “On closed shells in nuclei. II,” Phys. Rev. **75**, 1969 (1949).

[17] O. Haxel, J. H. D. Jensen, and H. E. Suess, “On the “magic numbers” in nuclear structure,” Phys. Rev. **75**, 1766 (1949).

[18] T. Schmidt, “Über die magnetischen Momente der Atomkerne,” Z. Phys. **106**, 358 (1937).

[19] L. W. Nordheim, “On spins, moments, and shells in nuclei,” Phys. Rev. **78**, 294 (1950).

[20] Evaluated Nuclear Structure Data File (ENSDF), National Nuclear Data Center, Brookhaven National Laboratory, `https://www.nndc.bnl.gov/ensdf/`.

[21] NuDat 3, National Nuclear Data Center, Brookhaven National Laboratory, `https://www.nndc.bnl.gov/nudat3/`.

[22] N. J. Stone, “Table of nuclear magnetic dipole and electric quadrupole moments,” At. Data Nucl. Data Tables **90**, 75 (2005); updated compilations at NNDC.

[23] W. N. Cottingham and D. A. Greenwood, *An Introduction to Nuclear Physics* (2nd ed.), Cambridge University Press, Cambridge (2001).

[24] H. Geiger and J. M. Nuttall, “The ranges of the α particles from the radioactive substances,” Phil. Mag. **22**, 613 (1911).

[25] G. Gamow, “Zur Quantentheorie des Atomkernes,” Z. Phys. **51**, 204 (1928).

[26] R. W. Gurney and E. U. Condon, “Wave mechanics and radioactive disintegration,” Nature **122**, 439 (1928); Phys. Rev. **33**, 127 (1929).

[27] M. Wang, W. J. Huang, F. G. Kondev, G. Audi, and S. Naimi, “The AME 2020 atomic mass evaluation (II). Tables, graphs and references,” Chin. Phys. C **45**, 030003 (2021).

[28] Laboratoire National Henri Becquerel (LNHB), Recommended decay data, `http://www.lnhb.fr/nuclear-data/nuclear-data-table/`.

[29] L. M. Langer, R. D. Moffat, and H. C. Price, Jr., “Low energy beta-ray spectra: P^{32} and Cu^{64},” Phys. Rev. **76**, 1725 (1949).

[30] L. M. Langer and H. C. Price, Jr., “Shapes of the beta-spectra of the forbidden transitions of Sb^{124}, Rb^{86}, Sr^{89}, Y^{91}, and Cs^{137},” Phys. Rev. **75**, 1769 (1949).

[31] D. C. Camp and L. M. Langer, “The shape of the ^{66}Ga positron spectrum and the contribution from $0^+ \to 0^+$ transitions,” Phys. Rev. **129**, 1782 (1963).

[32] H. C. Verma, *Nuclear Physics: Fundamentals and Applications*, NPTEL/IIT Kanpur lecture series, `https://hcverma.in/ncl_phy_lectures`.

[33] International Atomic Energy Agency, *LiveChart of Nuclides*, evaluated structure, decay, reaction, and fission-yield data, `https://www-nds.iaea.org/relnsd/vcharthtml/VChartHTML.html`.

[34] T. Kibédi, T. W. Burrows, M. B. Trzhaskovskaya, P. M. Davidson, and C. W. Nestor, Jr., "Evaluation of theoretical conversion coefficients using BrIcc," Nucl. Instrum. Methods Phys. Res. A **589**, 202 (2008), DOI: 10.1016/j.nima.2008.02.051.

[35] D. A. Brown *et al.*, "ENDF/B-VIII.0: The 8th major release of the nuclear reaction data library with CIELO-project cross sections, new standards and thermal scattering data," Nucl. Data Sheets **148**, 1 (2018), DOI: 10.1016/j.nds.2018.02.001.

[36] B. Acharya *et al.*, "Solar fusion III: New data and theory for hydrogen-burning stars," Rev. Mod. Phys. **97**, 035002 (2025), DOI: 10.1103/8lm7-gs18.

[37] S. N. Ghoshal, "An experimental verification of the theory of compound nucleus," Phys. Rev. **80**, 939 (1950), DOI: 10.1103/PhysRev.80.939.

[38] D. Adhikari *et al.* (PREX Collaboration), "Accurate determination of the neutron skin thickness of ^{208}Pb through parity-violation in electron scattering," Phys. Rev. Lett. **126**, 172502 (2021), DOI: 10.1103/PhysRevLett.126.172502.

[39] B. T. Reed, F. J. Fattoyev, C. J. Horowitz, and J. Piekarewicz, "Implications of PREX-II on the equation of state of neutron-rich matter," Phys. Rev. Lett. **126**, 172503 (2021), DOI: 10.1103/PhysRevLett.126.172503.

[40] B. Hu *et al.*, "Ab initio predictions link the neutron skin of ^{208}Pb to nuclear forces," Nature Phys. **18**, 1196 (2022), DOI: 10.1038/s41567-022-01715-8.

[41] E. Epelbaum, H.-W. Hammer, and U.-G. Meißner, "Modern theory of nuclear forces," Rev. Mod. Phys. **81**, 1773 (2009), DOI: 10.1103/RevModPhys.81.1773.

[42] H.-W. Hammer, S. König, and U. van Kolck, "Nuclear effective field theory: Status and perspectives," Rev. Mod. Phys. **92**, 025004 (2020), DOI: 10.1103/RevModPhys.92.025004.

[43] T. Otsuka, A. Gade, O. Sorlin, T. Suzuki, and Y. Utsuno, "Evolution of shell structure in exotic nuclei," Rev. Mod. Phys. **92**, 015002 (2020), DOI: 10.1103/RevModPhys.92.015002.

[44] H. Hergert, S. K. Bogner, T. D. Morris, A. Schwenk, and K. Tsukiyama, "The in-medium similarity renormalization group: A novel ab initio method for nuclei," Phys. Rep. **621**, 165 (2016), DOI: 10.1016/j.physrep.2015.12.007.

[45] J. M. Lattimer and M. Prakash, "The equation of state of hot, dense matter and neutron stars," Phys. Rep. **621**, 127 (2016), DOI: 10.1016/j.physrep.2015.12.005.

[46] J. M. Lattimer, "Neutron stars and the nuclear matter equation of state," Annu. Rev. Nucl. Part. Sci. **71**, 433 (2021), DOI: 10.1146/annurev-nucl-102419-124827.

[47] B. P. Abbott *et al.* (LIGO Scientific Collaboration and Virgo Collaboration), "GW170817: Observation of gravitational waves from a binary neutron star inspiral," Phys. Rev. Lett. **119**, 161101 (2017), DOI: 10.1103/PhysRevLett.119.161101.

[48] M. J. Dolinski, A. W. P. Poon, and W. Rodejohann, "Neutrinoless double-beta decay: Status and prospects," Annu. Rev. Nucl. Part. Sci. **69**, 219 (2019), DOI: 10.1146/annurev-nucl-101918-023407.

[49] M. Agostini, G. Benato, J. A. Detwiler, J. Menéndez, and F. Vissani, "Toward the discovery of matter creation with neutrinoless $\beta\beta$ decay," Rev. Mod. Phys. **95**, 025002 (2023), DOI: 10.1103/RevModPhys.95.025002.

[50] P. Gysbers *et al.*, "Discrepancy between experimental and theoretical β-decay rates resolved from first principles," Nature Phys. **15**, 428 (2019), DOI: 10.1038/s41567-019-0450-7.

[51] H. L. Crawford, K. Fossez, S. König, and A. Spyrou, "A vision for the science of rare isotopes," Annu. Rev. Nucl. Part. Sci. **74**, 141 (2024), DOI: 10.1146/annurev-nucl-121423-091501.

[52] Nuclear Science Advisory Committee, *A New Era of Discovery: The 2023 Long Range Plan for Nuclear Science*, U.S. Department of Energy and National Science Foundation (2023), `https://nuclearsciencefuture.org/`.

[53] S. A. Giuliani, Z. Matheson, W. Nazarewicz, E. Olsen, P.-G. Reinhard, J. Sadhukhan, B. Schuetrumpf, N. Schunck, and P. Schwerdtfeger, "Colloquium: Superheavy elements: Oganesson and beyond," Rev. Mod. Phys. **91**, 011001 (2019), DOI: 10.1103/RevModPhys.91.011001.

[54] N. Schunck and D. Regnier, "Theory of nuclear fission," Prog. Part. Nucl. Phys. **125**, 103963 (2022), DOI: 10.1016/j.ppnp.2022.103963.

[55] I. Counts, J. Hur, D. P. L. Aude Craik, H. Jeon, C. Leung, J. C. Berengut, A. Geddes, A. Kawasaki, W. Jhe, and V. Vuletić, "Evidence for nonlinear isotope shift in Yb^+ search for new boson," Phys. Rev. Lett. **125**, 123002 (2020), DOI: 10.1103/PhysRevLett.125.123002.

[56] I. Angeli and K. P. Marinova, "Table of experimental nuclear ground state charge radii: An update," At. Data Nucl. Data Tables **99**, 69 (2013), DOI: 10.1016/j.adt.2011.12.006.

[57] S. Kraemer *et al.*, "Observation of the radiative decay of the ^{229}Th nuclear clock isomer," Nature **617**, 706 (2023), DOI: 10.1038/s41586-023-05894-z.